Measurement and Modeling of Bias-Dependent Powder Cores Permeability

Measurement and Modeling of Bias-Dependent Powder Cores Permeability

Tommaso Bradde*, Arne Schröder†, Dierk Bormann‡, Alexandru Savca†, Stefano Grivet-Talocia*
*Dept. Electronics and Telecommunications, Politecnico di Torino, Italy,†Hitachi Energy Research, Switzerland,
‡Hitachi Energy Research, Sweden.
tommaso.bradde@polito.it

***Abstract*—This contribution treats the experimental and mathematical characterization of permeability spectra of magnetic powder materials subject to significant DC-current bias levels. The permeability spectra of two different commercial powder cores are experimentally measured and processed through two different modeling approaches, which allow exploiting the gathered data to properly predict the electrical behavior of high-frequency inductors built upon the considered magnetics, for the sake of system level simulation and optimization. The performance of the two approaches are compared and one example of EMI filter inductor design driven by the considered parameterized characterization is presented.**

I. Introduction

Optimizing magnetic components is essential for achieving the highest efficiency while minimizing size and costs of power converters and systems. Depending on the type of magnetic component and its application, various magnetic materials such as ferrites, powder cores, or nanocrystalline alloys are used. Whereas low-loss ferrites or nanocrystalline materials are usually employed in low-current applications (e.g. common mode chokes), powder cores are often preferred for high-current applications due to their superior saturation characteristics, low losses, and minimal hysteresis. For EMC compliance, such materials were successfully exploited for example in differential mode (DM) filters, see [1]. With the increasing need for low-voltage, high-power delivery in systems-on-chip, powder cores have been recently studied as candidate magnetics for integrated voltage regulators, as they can help meeting stringent design specifications [2].

When employed for filtering applications, coils built upon powder materials can experience significant low-frequency or DC currents, which partially saturates the magnetic material and change its permeability spectrum. As EMC analyses and optimization of power converters are generally performed based on transient simulations. High-frequency circuit representations of magnetic-based components including DC bias properties are important for effective system-level optimization. With the support of such predictions, designers can select the optimal characteristics, geometry and working condition of the involved magnetic materials. Moved by this opportunity, a (yet limited) number of contributions in the recent past were devoted to the problem of modeling the broadband permeability of powder cores with respect to the bias current level, see e.g. [3].

In this work, the broadband frequency spectra of two different commercial powder core materials are experimentally measured at different bias levels, and then modeled via a phenomenological [4] and a black-box approach [5], both aimed at reconstructing the measured data in terms of a mathematical description which admits an equivalent circuit representation based on bias-dependent elements. While the former approach is driven by physical considerations, the latter is fully behavioral and has the only purpose of providing the user with a passive macromodel reproducing the port behavior of the underlying component over the prescribed range of working conditions.

Our numerical results show that the phenomenological approach allows to reconstruct the measured data over a broad range of frequencies using only three fitting parameters whenever the target permeability spectrum does not exhibit dimensional resonances. When dimensional resonances occur, the black box approach grants better performance due to its less constrained and more tunable model structure, that comes at the price of slightly larger equivalent circuit models. The relevance of a proper bias-dependent permeability characterization for the considered materials is demonstrated over a simple coil design application.

II. Experimental Characterization

In this work, two commercial powder materials are taken into account. Their identifiers, properties and manufacturers are reported in Tab. I, where l_{e} denotes the core magnetic path length, A_{e} its effective cross section, A_L the (unbiased) inductance, B_{sat} the saturation flux density. For a given core, the complex permeability as a function of the DC bias overimposed DC bias I_{DC} can be expressed as

$$\mu_{\mathrm{r}}(\mathrm{j}\omega, I_{\mathrm{DC}}) = \mu'_{\mathrm{r}}(\omega, I_{\mathrm{DC}}) - \mathrm{j}\,\mu''_{\mathrm{r}}(\omega, I_{\mathrm{DC}})\,. \tag{1}$$

with ω the angular frequency and j the imaginary unit. The complex permeability spectra were obtained through impedance measurements of magnetic cores using the setup outlined in [4]. This setup utilizes shorted coaxial cavities that house the magnetic cores being studied. Unlike other commonly used setups that involve multiple turns around the cores, the setup used in this work can operate up to several hundred MHz without being affected by coil self-resonances. The permeability spectra were measured from $f_{\mathrm{min}} = 10$ kHz to $f_{\mathrm{max}} = 200$ MHz, with bias currents ranging

TABLE I
MAIN PROPERTIES OF CONSIDERED MAGNETIC POWDER CORES INVESTIGATED IN THIS WORK.

Material	***Mix 26***	***Kool Mμ* MAX**
Alloy	Fe	Fe-Si-Al
Core ID	T300-26	0079907A7
Manufact.	Micrometals	Magnetics
Initial μ_{r}	75	60
l_{e}	198 mm	196 mm
A_{e}	338 mm^2	221 mm^2
A_L	160 nH	85 nH
B_{sat}	1.38 T	1.0 T

from $I_{\text{min}} = 0$ A to $I_{\text{max}} = 2.5$ kA, corresponding to bias H fields between 0 Oe and 160 Oe for the selected core geometries.

For each of the magnetic cores under consideration, the experiments yield a set of permeability spectrum measurements, retrieved at discrete frequency-bias combinations. Introducing two indices $k = 1, \dots, K$ and $m = 1, \dots, M$, these measurements are denoted as:

$$\mu_{\text{r}}^{k,m} = \mu_{\text{r}}(\text{j}\omega^k, I_{\text{DC}}^m) \in \mathbb{C}, \tag{2}$$

where $\omega^k \in 2\pi[f_{\text{min}}, f_{\text{max}}]$ MHz and $I_{\text{DC}}^m \in [I_{\text{min}}, I_{\text{max}}]$ kA $\equiv \mathcal{I}$. Using (2), the impedance of an inductor made up of P stacked cores and N turns can be expressed as

$$Z^{k,m} = Z(\text{j}\omega^k, I_{\text{DC}}^m) = \text{j}\omega^k \mu_{\text{r}}^{k,m} \mu_0 \gamma \in \mathbb{C}, \tag{3}$$

where

$$\gamma = PN^2 \frac{A_e}{l_e} \tag{4}$$

is the geometry factor. Note that equation (3) does not account for parasitic inductive or capacitive effects due to the windings, that are not considered in this work.

III. BLACK BOX MODELING

The black-box modeling approach employed in this work is the one introduced in [5], which provides a general algorithm for generating guaranteed passive parameterized macromodels starting from the measurement set (3). Being s the Laplace variable, the method represents the macromodel in terms of its bias-dependent impedance $\hat{Z}(s, I_{\text{DC}})$, ensuring that it matches the coil impedance $Z(s, I_{\text{DC}})$ for every $I_{\text{DC}} \in \mathcal{I}$. This is achieved by utilizing the available measurements to enforce the approximation condition

$$\hat{Z}(\text{j}\omega^k, I_{\text{DC}}^m) \approx Z^{k,m}, \quad k = 1, \dots, K \quad m = 1, \dots, M, \tag{5}$$

relying on the barycentric model representation

$$\hat{Z}(s, I_{\text{DC}}) = \frac{\mathsf{N}(s, I_{\text{DC}})}{\mathsf{D}(s, I_{\text{DC}})} = \frac{\sum_{i=0}^{n} \sum_{\ell=0}^{\bar{\ell}} r_{i,\ell}\, b_\ell^{\bar{\ell}}(I_{\text{DC}}) \varphi_i(s)}{\sum_{i=0}^{n} \sum_{\ell=0}^{\bar{\ell}} p_{i,\ell}\, b_\ell^{\bar{\ell}}(I_{\text{DC}}) \varphi_i(s)}, \tag{6}$$

where

- $r_{i,\ell}, p_{i,\ell}$ are model coefficients to be optimized to enforce (5),
- $\varphi_i(s) = (s - q_i)^{-1}$ for $i = 1, \dots, n$ (with $\text{Re}(q_i) < 0$) are basis functions inducing the dependency on the Laplace variable. The basis $\varphi_0(s)$ is set to 1.
- The bias-dependent basis functions $b_\ell^{\bar{\ell}}(I_{\text{DC}})$ are the Bernstein polynomials of degree $\bar{\ell}$.

The barycentric model structure (6) admits an equivalent representation in terms of a proper transfer function of order n with poles, zeros, and direct coupling depending on the parameter I_{DC}. In particular, its poles and zeros are allowed to undergo bifurcations as I_{DC} varies.

The model coefficients $r_{i,\ell}, p_{i,\ell}$ are optimized so that (5) holds in least-squares sense. This is done applying the Parameterized Sanathanan-Koerner (PSK) algorithm [6], that iteratively solves a sequence of linearized and re-weighted linear least-squares problems. At iteration ν, the algorithm minimizes the cost function

$$E^\nu = \sum_{k=1}^{K} \sum_{m=1}^{M} \left\| \frac{\mathsf{N}^\nu(\text{j}\omega^k, I_{\text{DC}}^m) - \mathsf{D}^\nu(\text{j}\omega^k, I_{\text{DC}}^m) Z^{k,m}}{\mathsf{D}^{\nu-1}(\text{j}\omega^k, I_{\text{DC}}^m)} \right\|^2 \tag{7}$$

where the superscript ν indicates the model evaluated using the coefficient corresponding to the iteration ν, namely $r_{i,\ell}^\nu, p_{i,\ell}^\nu$. Given the initialization $\mathsf{D}^0(\text{j}\omega, I_{\text{DC}}) = 1$, the cost function (7) minimized at iteration ν is linear in such unknowns, as $\mathsf{D}^{\nu-1}$ can be evaluated numerically. The iteration terminates when

$$|E^\nu - E^{\nu-1}| < \epsilon \tag{8}$$

being ϵ a user defined positive threshold.

Straight minimization of E^ν does not guarantee that the final model corresponds to a stable and passive equivalent circuit for all bias current levels spanning $\mathcal{I}$. Hence, a constrained optimization approach must be pursued with the goal of minimizing (7) while guaranteeing these indispensable properties. In this view, the iterative minimization of the cost function E^ν is practically performed following the QR-based decoupling strategy introduced in [7], that allows estimating $r_{i,\ell}^\nu$ and $p_{i,\ell}^\nu$ in two successive steps, so that:

- the coefficients $p_{i,\ell}^\nu$ are first estimated under model asymptotic stability constraints. Full details of how such constraints are formulated are available in [5, Sec. IV].
- The coefficients $r_{i,\ell}^\nu$ are estimated by solving an unconstrained least-squares problem.

The above iterative procedure continues until (8) is met at iteration $\bar{\nu}$. Then an additional iteration is performed in which the ultimate numerator coefficients $r_{i,\ell}^{\bar{\nu}+1}$ are estimated again via constrained optimization that guarantees the model passivity uniformly over the parameter space. The formulation of the passivity constrained optimization problem is available in [5, Sec. V].

The model is then cast into a passive, behavioral equivalent circuit with element values explicitly parameterized by I_{DC}, which can be used to represent the coil in time or frequency domain system level simulations. The prediction of the core permeability spectrum for arbitrary I_{DC} is easily obtained by inverting relation (3) using the model response in place of the measurements.

IV. Phenomenological Model

The phenomenological model considered here for fitting the measured complex permeability spectra is an extension of the higher-order Debye approach introduced in [8] to the case in which I_{DC} is considered as a free parameter.

The underlying idea is that the magnetic grain response depends on a relaxation frequency ω_0 that can be assumed to be approximately equal to the frequency at which the magnetic skin depth is comparable with the grain dimension. An approximate relation can be given as

$$\omega_0 \approx \frac{4\pi^2}{\mu_{\text{ri}}\mu_0\sigma_{\text{i}}a_0^2}\,, \tag{9}$$

being μ_{ri} and σ_{i} the intrinsic relative permeability and electrical conductivity of the grain material, while a_0 is the grain diameter. The permeability spectrum of the grain below ω_0 response is essentially constant. At frequencies above ω_0, it is attenuated by the skin effect. Its dissipation maximum occurs at ω_0. This behavior is approximately represented by the Debye model

$$\chi(\mathrm{j}\omega) = \frac{1}{1+\mathrm{j}\omega/\omega_0}\,, \tag{10}$$

whose imaginary part attains a minimum at $\mathrm{j}\omega_0$, while the real part swings from 1 to 0 for increasing ω. When many grains of different size are subject to variable bias field, the relative permeability $\mu_{\text{r}}(\mathrm{j}\omega, I_{\text{DC}})$ can be assumed to obey the following scaling form, introduced in [4]:

$$\mu_{\text{r}}(\mathrm{j}\omega, I_{\text{DC}}) = \mu_{\text{r}}(0, I_{\text{DC}})F_\lambda\left(\frac{\mathrm{j}\omega}{\omega_{\text{cro}}(I_{\text{DC}})}\right)\,, \tag{11}$$

where ω_{cro} reads

$$\omega_{\text{cro}}(I_{\text{DC}}) = \omega_0\left[\frac{\mu_{\text{r}}(0, I_{\text{DC}})}{\mu_{\text{r}}(0,0)}\right]^{-\beta} \tag{12}$$

and represents the bias-dependent "crossover frequency" at which $\mu_{\text{r}}''(\omega, I_{\text{DC}})$ has its maximum. In (12), β is a scaling exponent, and the dimensionless scaling function F_λ is defined as

$$F_\lambda(\mathrm{j}x) = \frac{1}{\sqrt{2\pi\lambda}}\int_{-\infty}^{\infty}\frac{\mathrm{e}^{-t^2/2\lambda}}{1+\mathrm{e}^t\mathrm{j}x}\mathrm{d}t\,. \tag{13}$$

The integral represents an averaging over t of the core grain sizes, performed assuming a log-normal distribution with variance λ for grains with diameter $a = \mathrm{e}^t a_0$. See [4] for further technical details.

In practice, the integral defining F_λ is replaced by a finite sum of n discrete values of t, symmetrically placed around 0 combined through appropriate Gaussian weights. This approach returns a function $\mu_{\text{r}}(\mathrm{j}\omega, I_{\text{DC}})$ with n poles, for which a Foster equivalent circuit can be obtained as in [4].

Since the values of static bias-dependent permeability $\mu_{\text{r}}(0, I_{\text{DC}})$ can be extracted directly from the low-frequency behavior of the observed data, the employed phenomenological modeling procedure consists of determining only three free parameters, namely the zero-bias crossover frequency $\omega_0 = 2\pi f_0$, the variance λ of the log-normal grain size distribution, and the bias scaling exponent β. Contrarily to what is done in the black-box approach of Sec. III this approach does not use the poles and residues locations as independent fitting parameters. All the electrical properties of the resulting equivalent circuit depend on the three above mentioned fitting parameters and on the number n used to perform integral discretization.

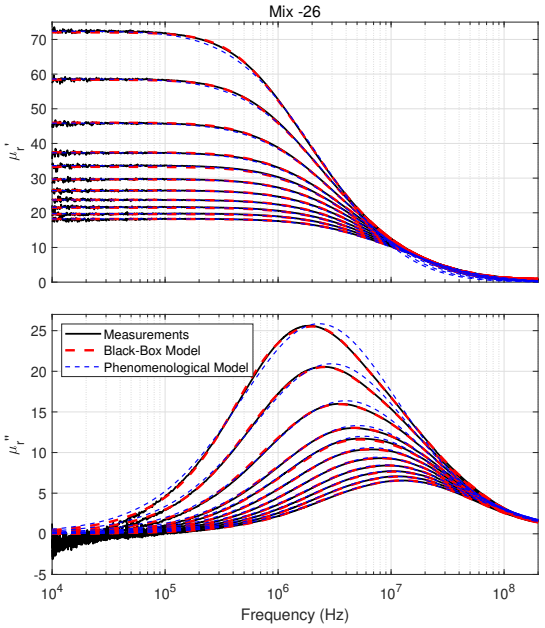

Fig. 1. *Mix -26* material. Measured and reconstructed permeability spectra. Each curve is related to a fixed H-field, ranging from 0 Oe, to 157 Oe. As the field intensity increases, the low frequency value of μ_{r}' decreases.

V. Numerical Results

We applied the modeling schemes recalled in Sections III and IV to the available measurements using the modeling settings reported in Table II.

TABLE II

Fitting Parameter	Black-Box Model n	Black-Box Model $\bar{\ell}$	Phenomenological Model f_0 (MHz)	Phenomenological Model λ	Phenomenological Model β
Mix -26	9	4	2.3	0.34	1.2
Kool Mμ MAX	8	4	10	0.80	1.0

The modeling results for the *Mix -26* material are shown in Fig. 1. Both methods reconstruct the data with remarkable accuracy: the Root Mean Square (RMS) error (computed over all available measurements) amounts to 4.90% and 1.38% for the phenomenological and behavioral models, respectively. The former is expected to perform satisfactorily as the permeability shows a standard relaxation behavior.

Different conclusions can be drawn when using the two approaches to model the permeability of the *Kool Mμ MAX* core. The permeability of this material is characterized by significant dimensional resonances and by a negative real part in the MHz frequency range. Whereas the accuracy of the

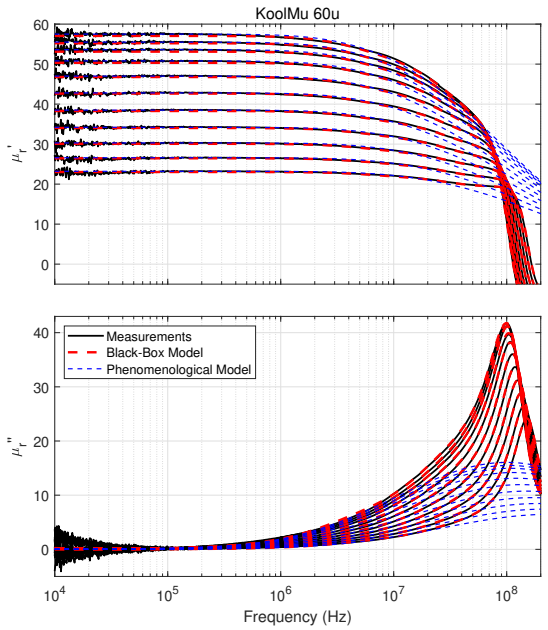

Fig. 2. Measured and fitted complex permeability spectra as in Fig. 1 but for the material *Kool Mμ MAX*. For this kind of material, the phenomenological approach fails to reconstruct the high-frequency measurements due to the dimensional resonance.

behavioral model is in full agreement with that of the previous core, the fitting obtained with the phenomenological approach is very accurate only up to 10 MHz; at higher frequencies, the model fails to capture the dimensional resonance. As a consequence, the RMS error committed by the latter modeling strategy is about one order of magnitude larger than that of the former (12.33% against 1.29%).

The modeled permeability spectra are important of system-level analyses as shown next. We consider a generic converter high-frequency model, consisting of a multiport RLCG network. To model the switching events, one port of the network is closed over a noise voltage source with broadband spectrum and amplitude of 1 V. A high-amplitude, low-frequency current is assumed to flow from the input to the output port of the converter. These ports are shunted by two high-frequency terminations that provide a path to ground for high-frequency currents. The objective is to include in the converter design two EMI filters that minimize the amplitude of the high-frequency current that flows through the converter looping via the high-frequency terminations. To this end, we include in the converter design a pair of identical EMI filters composed of a single-turn inductor including the *Kool MμMAX* powder core. The inductance of the coils is $L_{\text{Filt}} = 1.3\,\mu\text{H}$ at 0 Oe. The response of the converter to an excitation of bandwidth 10 MHz, with and without EMI filters, is shown in Fig. 3. If no filters are used, significant current components are present above 4 MHz, with peak amplitude arising at 6 MHz. Such resonances are attenuated by the EMI filters. Due to the high-amplitude current flowing into the converter, the filtering effect depends on the bias current level, i.e., on the converter operating condition. for the considered example, the filter grants an attenuation of 20 dB when the bias amounts to 0 Oe. For a 150 Oe bias, the attenuation is reduced to 10 dB. As expected, the influence of the bias level on the system performance is significant and motivates the need for accurate characterization of bias dependent magnetic components.

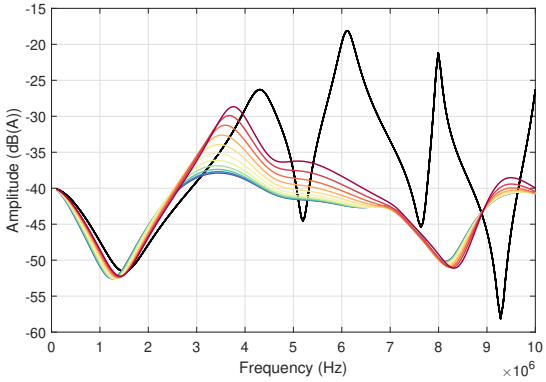

Fig. 3. High-frequency current response of the converter to a 1 V broadband excitation. Black line: response of the converter without EMI filters. Colored lines: with EMI filters and different bias levels, denoted by the line colors from blue (0 Oe) to red (150 Oe).

VI. Conclusions

In this contribution, the permeability spectra of commercial powder cores are characterized both in terms of measurements and mathematical models. Our results show that the effect of high magnetizing fields are relevant for assessing the performance of this kind of cores when they are used in high-current applications. Hence, accurate equivalent circuits that properly reproduce such dependency represent a critical asset for meaningful system level analysis and design.

References

[1] D. O. Boillat, F. Krismer, and J. W. Kolar, "EMI filter volume minimization of a three-phase, three-level T-type PWM converter system," *IEEE Transactions on Power Electronics*, vol. 32, no. 4, pp. 2473–2480, 2017.

[2] S. S. A. Venkataramanan, P. Murali, D. A. Gilbert, M. Kathaperumal, and M. D. Losego, "Magnetic cores for high conversion ratio package embedded inductors," in *2024 IEEE 74th Electronic Components and Technology Conference (ECTC)*, 2024, pp. 2250–2255.

[3] P. Leszczynski, K. Kutorasinski, M. Szewczyk, and J. Pawłowski, "Machine-learned models for power magnetic material characteristics," *IEEE Transactions on Power Electronics*, pp. 1–9, 2024.

[4] A. Schroeder, A. Savca, and D. Bormann, "High frequency permeability measurements and modeling of magnetic powder cores under DC bias," *submitted to IEEE Transactions on Power Electronics*, 2024.

[5] T. Bradde, S. Grivet-Talocia, A. Zanco, and G. C. Calafiore, "Data-driven extraction of uniformly stable and passive parameterized macromodels," *IEEE Access*, vol. 10, pp. 15 786–15 804, 2022.

[6] D. Deschrijver, T. Dhaene, and D. De Zutter, "Robust parametric macromodeling using multivariate orthonormal vector fitting," *IEEE Transactions on Microwave Theory and Techniques*, vol. 56, no. 7, pp. 1661–1667, 2008.

[7] T. Bradde, S. Grivet-Talocia, M. De Stefano, and A. Zanco, "A scalable reduced-order modeling algorithm for the construction of parameterized interconnect macromodels from scattering responses," in *proc. IEEE Symp. Electromag. Compat. Signal Integrity Power Integrity*. Long Beach, CA, USA: IEEE, 2018, pp. 650–655.

[8] X. Liu, F. Grassi, G. Spadacini, S. A. Pignari, F. Trotti, N. Mora, and W. Hirschi, "Behavioral modeling of complex magnetic permeability with high-order debye model and equivalent circuits," *IEEE Transactions on Electromagnetic Compatibility*, vol. 63, no. 3, pp. 730–738, 2021.